Unscented Dual Quaternion Particle Filter for SE(3) Estimation

Kailai Li, *Graduate Student Member, IEEE*, Florian Pfaff, *Member, IEEE*, and Uwe D. Hanebeck, *Fellow, IEEE*

***Abstract*—We present a novel dual quaternion filter for recursive estimation of rigid body motions. Based on the sequential Monte Carlo scheme, particles are deployed on the manifold of unit dual quaternions. This allows nonparametric modeling of arbitrary distributions underlying on the SE(3) group. The proposal distribution for importance sampling is estimated particle-wise by a novel dual quaternion unscented Kalman filter (DQ-UKF). It is adapted to the manifold geometric structure and drives the prior particles towards high-likelihood regions on the manifold. The resultant unscented dual quaternion particle filter (U-DQPF) incorporates the most recently observed evidence, raising the particle efficiency considerably for nonlinear pose estimation tasks. Compared with ordinary particle filters and other parametric model-based dual quaternion filtering schemes, the proposed U-DQPF shows superior performance in nonlinear SE(3) estimation.**

***Index Terms*—Filtering, estimation, sensor fusion.**

I. Introduction

SPATIAL pose estimation is crucial in many control-related scenarios [1]–[4]. Mathematically speaking, rigid body motions, which incorporate both rotation and translation, can be described by the elements belonging to the special Euclidean group SE(3). For SE(3) estimation, there exist several different representations of the states. Minimal representations of spatial rotations typically suffer from singularities or discontinuities for certain attitudes (e.g., the "gimbal lock" issue with Euler angles). The widely used 4×4 homogeneous matrices eliminate such issues via overparameterization, however, with a large degree of redundancy (w.r.t. the six DoF), leading to memory inefficiency and numerical instabilities. A dual quaternion comprises two quaternions, and thus, it can be expressed as an eight-dimensional vector, inducing only two degrees of redundancy and no singularity. Therefore, we employ dual quaternions as state representation in the proposed rigid body motion estimator.

Due to the nonlinear group structure of SE(3), existing pose estimation methods often assume local perturbations on the underlying group (e.g., via Lie algebra) [3]–[5]. This enables nonlinear state estimation in a locally linearized space using popular filtering schemes such as the extended Kalman filter (EKF) or the unscented Kalman filter (UKF) [6], [7]. The SE(3) states are often augmented by vectors describing the velocities or accelerations, which demand additional inertial systems of a high sampling rate. Such an assumption can be invalid for scenarios without extra motion information, e.g., for pose estimation purely based on external perception sensors [8]–[10]. Furthermore, the assumption can be also easily violated when there are large transitions and high uncertainties with system dynamics. Consequently, the estimated uncertainty (e.g., quantified by a Gaussian distribution) in the locally linearized space can be warped with a distorted shape on SE(3) by the exponential map, and thus, does not correspond to the geodesic distance and has a questionable interpretation. Dual quaternions representing uncertain rigid body motions naturally form a nonlinear manifold in $\mathbb{R}^8$ (see Section II). In this letter, we focus on the conceptual scenario where dual quaternion SE(3) states are to be estimated adaptively to its inherent manifold geometry.

The nonlinear structure of the dual quaternion manifold results from the rotational component represented by unit quaternions, which are located on the unit hypersphere $\mathbb{S}^3$. Thus, significant effort has been devoted to applying distributions from directional statistics [11], [12] to stochastic modeling of uncertain unit quaternions directly on the hypersphere without linearization. A quaternion $\mathbf{x}_\mathrm{r} \in \mathbb{S}^3$ and its antipode $-\mathbf{x}_\mathrm{r}$ represent the same rotation, thus should be endowed with identical density values. Therefore, Bingham distribution in $\mathbb{R}^4$ has gained popularity as its density is inherently antipodally symmetric on $\mathbb{S}^3$. In [10], the Bingham distribution was used for Monte Carlo-based orientation estimation. An unscented orientation estimator was proposed in [13] based on a deterministic sampling scheme for the Bingham distribution. It showed superior tracking accuracy and less runtime than an ordinary UKF-based quaternion filter.

Further extensions were made for modeling uncertain dual quaternions based on hyperspherical distributions. In [8],

Manuscript received March 17, 2020; revised May 30, 2020; accepted June 19, 2020. Date of publication June 25, 2020; date of current version July 9, 2020. This work was supported by the German Research Foundation (DFG) under Grant HA 3789/16-1. Recommended by Senior Editor V. Ugrinovskii. *(Corresponding author: Kailai Li.)*

The authors are with the Intelligent Sensor-Actuator-Systems Laboratory, Institute for Anthropomatics and Robotics, Karlsruhe Institute of Technology, 76131 Karlsruhe, Germany (e-mail: kailai.li@kit.edu; florian.pfaff@kit.edu; uwe.hanebeck@kit.edu).

Digital Object Identifier 10.1109/LCSYS.2020.3005066

Bingham-distributed quaternions and Gaussian-distributed translation terms are combined in an unscented transform-based dual quaternion filter for visual odometry. A Bingham-based linear filter was proposed in [14] for static point cloud registration using the dual quaternion representation and pseudo-measurements of vertex-pairs. Further parametric schemes were established in [15]–[18], in which uncertain dual quaternions are modeled in a unified way for pose estimation and methods were facilitated with deterministic or stochastic sampling. Several issues arise in parametric statistical modeling on the manifold of dual quaternions. First, almost no relevant hyperspherical distribution possesses a normalization constant in closed form. Some techniques were introduced for accelerating the computation, e.g., using lookup tables or saddle points for the Bingham distribution [13], [19], yet they are still time-consuming and sometimes numerically unstable due to numerical optimizations or approximations. Some models assume low rotation uncertainty and need complex mixture models for handling high uncertainties [17], [18].

Particularly, parametric statistical models deny exact modeling of arbitrary distributions on the nonlinear manifold. Considering that the unit quaternion manifold is bounded and compact, a discrete quaternion filter was proposed in [20] using a hyperspherical grid, which allows approximating arbitrary distributions. Based thereon, it is possible to incorporate translations into dual quaternion representation via Rao–Blackwellization for pose estimation [21]. However, the major limitation lies in the uniform or non-adaptive discretization, which leads to a large grid resolution for nonlinear filtering. This results in a high computational and storage complexity.

Theoretically, Monte Carlo schemes are applicable for exact modeling of arbitrary distributions. In practice, however, a plain dual quaternion particle filter (PF) may suffer from sample degeneration due to nonlinearities and high-dimensional state spaces, thereby demanding a large number of particles for nonlinear SE(3) estimation. Moreover, standard PFs exploit the transition density as the proposal distribution, and thus, newly observed evidence from current measurement is disregarded. This may lead to deteriorated estimation performance with peaky likelihoods, non-stationary models, as well as heavy-tailed distributions, etc. In this regard, the unscented particle filter (UPF), in which each particle runs an individual UKF to estimate the proposal distribution, was proposed in [22]. It has been systematically justified that a theoretical convergence is ensured with the UPF and its convergence rate is dimension-independent. Consequently, it shows substantial improvements over standard PFs for nonlinear state estimation. By far, there exists no such scheme for dual quaternion filtering.

Contributions: We establish a geometry-aware UPF scheme on the manifold of unit dual quaternions for nonlinear SE(3) estimation. An investigation into the geometric structure of the manifold is provided. Afterward, random dual quaternion particles are exploited for exact on-manifold modeling of arbitrary distributions. The concept of locally augmented tangent space (LATS) is introduced based on augmented gnomonic projection/retraction to facilitate a novel UKF-like dual quaternion filter (DQ-UKF). Then, the proposal distribution is estimated particle-wise by the DQ-UKF such that the latest evidence is fused before importance sampling. The resultant unscented dual quaternion particle filter (U-DQPF), as demonstrated in evaluation, shows superior performance over the PF and the Bingham-based dual quaternion filter.

II. Preliminaries

A. Quaternion Representation of Spatial Rotations

By convention, a quaternion $\mathbf{r}$ is defined as $r_0 + r_1\mathbf{i} + r_2\mathbf{j} + r_3\mathbf{k}$. The set $\{\mathbf{i}, \mathbf{j}, \mathbf{k}\}$ is the standard basis of the three-dimensional Euclidean space $\mathbb{R}^3$, following Hamilton product $\otimes$ in quaternion composition. For conciseness, we rewrite quaternions into vector form with $\mathbf{r} = [r_0, r_1, r_2, r_3]^\top \in \mathbb{R}^4$. The composition of two arbitrary quaternions $\mathbf{r}$ and $\mathbf{s}$ can then be reformulated into ordinary matrix–vector multiplications, namely $\mathbf{r} \otimes \mathbf{s} = \mathcal{Q}_{\mathbf{r}}^{\llcorner} \mathbf{s} = \mathcal{Q}_{\mathbf{s}}^{\lrcorner} \mathbf{r}$, with

$$\mathcal{Q}_{\mathbf{r}}^{\llcorner} = \begin{bmatrix} r_0 & -r_1 & -r_2 & -r_3 \\ r_1 & r_0 & -r_3 & r_2 \\ r_2 & r_3 & r_0 & -r_1 \\ r_3 & -r_2 & r_1 & r_0 \end{bmatrix}, \quad \mathcal{Q}_{\mathbf{s}}^{\lrcorner} = \begin{bmatrix} s_0 & -s_1 & -s_2 & -s_3 \\ s_1 & s_0 & s_3 & -s_2 \\ s_2 & -s_3 & s_0 & s_1 \\ s_3 & s_2 & -s_1 & s_0 \end{bmatrix}. \quad (1)$$

The norm of a quaternion $\mathbf{r}$ is defined as $\sqrt{\mathbf{r} \otimes \mathbf{r}^*}$, with $\mathbf{r}^* = [r_0, -r_1, -r_2, -r_3]^\top$ being the conjugate of $\mathbf{r}$. Quaternions of unit norm are called unit quaternions. They are also of unit length in the four-dimensional Euclidean space, thereby located on the unit hypersphere $\mathbb{S}^3 \subset \mathbb{R}^4$.

Given an arbitrary unit quaternion $\mathbf{r} \in \mathbb{S}^3$, it can be proven that its corresponding matrices in (1) belong to the four-dimensional special orthogonal group SO(4), namely $\mathcal{Q}_{\mathbf{r}}^{\circ}(\mathcal{Q}_{\mathbf{r}}^{\circ})^\top = (\mathcal{Q}_{\mathbf{r}}^{\circ})^\top \mathcal{Q}_{\mathbf{r}}^{\circ} = \mathbf{I}_{4\times4}$ and $\det(\mathcal{Q}_{\mathbf{r}}^{\circ}) = 1$ (superscript $\circ$ denotes either $\llcorner$ or $\lrcorner$). For unit quaternions, therefore, the Hamilton product denotes hyperspherical rotations geometrically, under which $\mathbb{S}^3$ is closed. Given the definition of quaternion norm, the inverse of a unit quaternion $\mathbf{r}$ equals its conjugate with $\mathbf{r}^{-1} = \mathbf{r}^*$, which corresponds to the inverse of its matrix expression, i.e., $\mathcal{Q}_{\mathbf{r}^{-1}}^{\circ} = (\mathcal{Q}_{\mathbf{r}}^{\circ})^\top = (\mathcal{Q}_{\mathbf{r}}^{\circ})^{-1}$.

Quaternions are popular for representing spatial rotations. A rotation of angle θ around the axis $\mathbf{n} \in \mathbb{S}^2$ can be parameterized by a quaternion of the following form

$$\mathbf{x}_\mathrm{r} = [\cos(\theta/2), \mathbf{n}^\top \sin(\theta/2)]^\top. \quad (2)$$

As the rotation axis denotes a unit vector in $\mathbb{R}^3$, the quaternion described above is naturally of unit norm, thereby $\mathbf{x}_\mathrm{r} \in \mathbb{S}^3$. It can rotate any point $\mathbf{p} \in \mathbb{R}^3$ to $\mathbf{p}'$ via $\mathbf{p}' = (\mathbf{x}_\mathrm{r} \otimes [0, \mathbf{p}^\top]^\top \otimes \mathbf{x}_\mathrm{r}^*)_{2:4}$. Here, we augment the vector $\mathbf{p}$ to its quaternion form and recover its coordinates by extracting the last three elements after the quaternion rotation. When applying the matrix expression in (1) to the unit quaternion $\mathbf{x}_\mathrm{r}$, one can establish the connection between quaternion rotation and the special orthogonal group SO(3). Since $\mathbf{x}_\mathrm{r} \otimes [0, \mathbf{p}^\top]^\top \otimes \mathbf{x}_\mathrm{r}^* = (\mathcal{Q}_{\mathbf{x}_\mathrm{r}}^{\lrcorner})^\top \mathcal{Q}_{\mathbf{x}_\mathrm{r}}^{\llcorner} [0, \mathbf{p}^\top]^\top$, we obtain $(\mathcal{Q}_{\mathbf{x}_\mathrm{r}}^{\lrcorner})^\top \mathcal{Q}_{\mathbf{x}_\mathrm{r}}^{\llcorner} = \begin{bmatrix} 1 & \mathbf{0}_{3\times1} \\ \mathbf{0}_{1\times3} & \mathcal{R}_{\mathbf{x}_\mathrm{r}} \end{bmatrix}$. $\mathcal{R}_{\mathbf{x}_\mathrm{r}} \in \mathrm{SO}(3)$ is the well-known rotation matrix denoting an identical spatial rotation as $\mathbf{x}_\mathrm{r}$.

B. Dual Quaternion-Based Pose Representation

To represent rigid body motions, a dual quaternion $\mathbf{x} = \mathbf{x}_\mathrm{r} + \epsilon\, \mathbf{x}_\mathrm{s}$ can be deployed with the real part $\mathbf{x}_\mathrm{r}$ explained in (2) and the dual part $\mathbf{x}_\mathrm{s}$ defined as

$$\mathbf{x}_\mathrm{s} = 0.5\, [0, \mathbf{t}^\top]^\top \otimes \mathbf{x}_\mathrm{r} \in \mathbb{R}^4. \quad (3)$$

Here, $\mathbf{x}_\mathrm{s}$ encodes the spatial translation $\mathbf{t} \in \mathbb{R}^3$ by aggregating $\mathbf{t}$ with the real part $\mathbf{x}_\mathrm{r}$. ϵ is the dual unit and satisfies $\epsilon^2 = 0$. Based thereon, we denote dual quaternions as eight-dimensional vectors by concatenating the real and dual parts together, namely $\mathbf{x} = [\mathbf{x}_\mathrm{r}^\top, \mathbf{x}_\mathrm{s}^\top]^\top$. The arithmetic of dual quaternion is a combination of quaternion arithmetic and dual number theory (due to the dual unit ϵ). Dual quaternion compositions, denoted by $\boxplus$, can be expressed as matrix–vector multiplications. For instance, we have $\mathbf{x} \boxplus \mathbf{y} = \mathcal{Q}_\mathbf{x}^\ulcorner \mathbf{y} = \mathcal{Q}_\mathbf{y}^\urcorner \mathbf{x}$ for two arbitrary dual quaternions $\mathbf{x} = [\mathbf{x}_\mathrm{r}^\top, \mathbf{x}_\mathrm{s}^\top]^\top$, $\mathbf{y} = [\mathbf{y}_\mathrm{r}^\top, \mathbf{y}_\mathrm{s}^\top]^\top \in \mathbb{R}^8$, with

$$\mathcal{Q}_\mathbf{x}^\ulcorner = \begin{bmatrix} \mathcal{Q}_{\mathbf{x}_\mathrm{r}}^\llcorner & \mathbf{0}_{4\times4} \\ \mathcal{Q}_{\mathbf{x}_\mathrm{s}}^\llcorner & \mathcal{Q}_{\mathbf{x}_\mathrm{r}}^\llcorner \end{bmatrix}, \quad \mathcal{Q}_\mathbf{y}^\urcorner = \begin{bmatrix} \mathcal{Q}_{\mathbf{y}_\mathrm{r}}^\lrcorner & \mathbf{0}_{4\times4} \\ \mathcal{Q}_{\mathbf{y}_\mathrm{s}}^\lrcorner & \mathcal{Q}_{\mathbf{y}_\mathrm{r}}^\lrcorner \end{bmatrix}.$$

As for quaternions, the norm of a dual quaternion is given by $\sqrt{\mathbf{x} \boxplus \mathbf{x}^*}$, with $\mathbf{x}^* = [(\mathbf{x}_\mathrm{r}^*)^\top, (\mathbf{x}_\mathrm{s}^*)^\top]^\top$ being the so-called classic conjugate of $\mathbf{x}$ [16].

Given the definition in (2) and (3), any point $\mathbf{p} \in \mathbb{R}^3$ can be transformed by a dual quaternion $\mathbf{x}$ according to $\mathbf{p}' = (\mathbf{x} \boxplus [1, 0, 0, 0, 0, \mathbf{p}]^\top \boxplus \mathbf{x}^\odot)_{6:8}$, with $\mathbf{x}^\odot = [(\mathbf{x}_\mathrm{r}^*)^\top, (-\mathbf{x}_\mathrm{s}^*)^\top]^\top$ being the full conjugate of $\mathbf{x}$. We augment $\mathbf{p}$ into a dual quaternion expression and extract the last three entries (6th to 8th) of the resultant dual quaternion to obtain its transformed coordinates. The transformation essentially denotes a rotation of $\mathbf{x}_\mathrm{r}$ followed by a translation of $\mathbf{t}$, i.e., $\mathbf{p}' = (\mathbf{x}_\mathrm{r} \otimes [0, \mathbf{p}^\top]^\top \otimes \mathbf{x}_\mathrm{r}^*)_{2:4} + \mathbf{t}$ [16].

C. Manifold Structure of Unit Dual Quaternions

Dual quaternions representing the SE(3) states in (3) are inherently of unit norm [23] and are thus called unit dual quaternions. As mentioned in Section II-A, real parts representing rotations are located on the unit hypersphere $\mathbb{S}^3$. Due to the Hamilton product in (3), the dual part is orthogonal to the real part on $\mathbb{S}^3$. Thus, we obtain the unit dual quaternion manifold $\mathbb{DH}_1 := \{[\mathbf{x}_\mathrm{r}^\top, \mathbf{x}_\mathrm{s}^\top]^\top \,|\, \mathbf{x}_\mathrm{r} \in \mathbb{S}^3, \mathbf{x}_\mathrm{r}^\top \mathbf{x}_\mathrm{s} = 0\} \subset \mathbb{R}^8$.

Furthermore, for a unit quaternion $\mathbf{x}_\mathrm{r} \in \mathbb{S}^3$, the matrix expression in (1) naturally provides an orthogonal basis of the four-dimensional Euclidean space $\mathbb{R}^4$. More specifically, its last three columns span the tangent space of the unit quaternion manifold at $\mathbf{x}_\mathrm{r}$, namely, $\mathbb{T}_{\mathbf{x}_\mathrm{r}}\mathbb{S}^3 = \mathrm{span}(\{\mathbf{e}_1, \mathbf{e}_2, \mathbf{e}_3\})$. Here, we decompose the matrix $\mathcal{Q}_{\mathbf{x}_\mathrm{r}}^\circ$ as $\mathcal{Q}_{\mathbf{x}_\mathrm{r}}^\circ = [\mathbf{x}_\mathrm{r}, \mathcal{A}_{\mathbf{x}_\mathrm{r}}^\circ]$, with $\mathcal{A}_{\mathbf{x}_\mathrm{r}}^\circ = [\mathbf{e}_1, \mathbf{e}_2, \mathbf{e}_3] \in \mathbb{R}^{4\times3}$. Then, the dual part $\mathbf{x}_\mathrm{s}$ defined in (3) is a scaled translation term w.r.t. the local basis $\mathcal{A}_{\mathbf{x}_\mathrm{r}}^\circ$ of $\mathbb{T}_{\mathbf{x}_\mathrm{r}}\mathbb{S}^3$. Therefore, we have $\mathbf{x}_\mathrm{s} = 0.5\,[0, \mathbf{t}^\top]^\top \otimes \mathbf{x}_\mathrm{r} = 0.5\,\mathcal{Q}_{\mathbf{x}_\mathrm{r}}^\lrcorner [0, \mathbf{t}^\top]^\top = 0.5\,\mathcal{A}_{\mathbf{x}_\mathrm{r}}^\lrcorner \mathbf{t}$. Since $\mathcal{A}_{\mathbf{x}_\mathrm{r}}^{\lrcorner\top} \mathcal{A}_{\mathbf{x}_\mathrm{r}}^\lrcorner = \mathbf{I}_{3\times3}$, the translation $\mathbf{t}$ can be decoded from the dual part via

$$\mathbf{t} = (2\,\mathbf{x}_\mathrm{s} \otimes \mathbf{x}_\mathrm{r}^{-1})_{2:4} = 2\mathcal{A}_{\mathbf{x}_\mathrm{r}}^{\lrcorner\top} \mathbf{x}_\mathrm{s}. \tag{4}$$

III. Geometric-Adaptive Stochastic Modeling for Uncertain Unit Dual Quaternions

A. Sequential Monte Carlo Scheme on $\mathbb{DH}_1$

The following setup is considered for dual quaternion filtering. The system model is $\mathbf{x}_k = a(\mathbf{x}_{k-1}, \mathbf{w}_{k-1})$, with the dual quaternion vectors $\mathbf{x}_{k-1}, \mathbf{x}_k \in \mathbb{DH}_1$ representing the SE(3) states and $\mathbf{w}_{k-1} \in \mathbb{W}$ being the system noise. The measurement model is $\mathbf{z}_k = h(\mathbf{x}_k, \mathbf{v}_k)$, with $\mathbf{z}_k \in \mathbb{Z}$ denoting the measurement and $\mathbf{v}_k \in \mathbb{V}$ the measurement noise. Note that neither the transition $a : \mathbb{DH}_1 \times \mathbb{W} \to \mathbb{DH}_1$ nor the observation $h : \mathbb{DH}_1 \times \mathbb{V} \to \mathbb{Z}$ is assumed to be of a specific class of functions (e.g., identity models in [13]).

Following a typical particle filtering scheme [24], we exploit Dirac mixtures supported by dual quaternion particles to represent the underlying posterior distribution on $\mathbb{DH}_1$. Thus, $f(\mathbf{x}_{0:k} \,|\, \mathbf{z}_{0:k}) = \sum_{i=1}^n w_k^i\, \delta(\mathbf{x}_{0:k} - \boldsymbol{\nu}_k^i)$, where w_k^i is the weight of each particle $\boldsymbol{\nu}_k^i \in \mathbb{DH}_1$ at step k and $\sum_{i=1}^n w_k^i = 1$. Theoretically, sampling particles from the true posterior density is infeasible. Instead, samples are drawn from the proposal distribution $g(\mathbf{x}_k^i \,|\, \mathbf{x}_{0:k-1}^i, \mathbf{z}_{1:k})$. It is a known distribution that is easy to sample such that the importance weight of each particle i can be recursively updated following

$$w_k^i = w_{k-1}^i \frac{f^\mathrm{L}(\mathbf{z}_k \,|\, \mathbf{x}_k^i) f^\mathrm{T}(\mathbf{x}_k^i \,|\, \mathbf{x}_{k-1}^i)}{g(\mathbf{x}_k^i \,|\, \mathbf{x}_{0:k-1}^i, \mathbf{z}_{1:k})}. \tag{5}$$

Standard PFs set the proposal distribution identical to the transition density, i.e., $g(\mathbf{x}_k^i \,|\, \mathbf{x}_{0:k-1}^i, \mathbf{z}_{1:k}) = f^\mathrm{T}(\mathbf{x}_k^i \,|\, \mathbf{x}_{k-1}^i)$, leading to an update merely done by the likelihood with $w_k^i = w_{k-1}^i f^\mathrm{L}(\mathbf{z}_k \,|\, \mathbf{x}_k^i)$. The latest evidence $\mathbf{z}_k$ is then disregarded from the proposal distribution, resulting in sample degeneration in the presence of, e.g., heavy-tailed distributions, non-stationary models, peaky likelihoods, etc. Inspired by [22] and considering the manifold structure, we propose a UKF-like dual quaternion filter on $\mathbb{DH}_1$ for particle-wise estimation of the proposal distribution.

B. Particle-Wise Probabilistic Modeling in the Locally Augmented Tangent Space

As detailed in Section II-C, the nonlinearity of the manifold $\mathbb{DH}_1$ mostly results from the real part on $\mathbb{S}^3$. Any unit quaternion $\mathbf{x}_\mathrm{r} \in \mathbb{S}^3$ can be mapped to the tangent space at another unit quaternion $\boldsymbol{\nu}_\mathrm{r} \in \mathbb{S}^3$ and backward via the gnomonic projection and retraction

$$\tilde{\mathbf{x}}_\mathrm{r} = \mathbf{x}_\mathrm{r}/(\boldsymbol{\nu}_\mathrm{r}^\top \mathbf{x}_\mathrm{r}) \in \mathbb{T}_{\boldsymbol{\nu}_\mathrm{r}}\mathbb{S}^3,\ \forall\, \mathbf{x}_\mathrm{r} \in \mathbb{S}^3,$$
$$\mathbf{x}_\mathrm{r} = \tilde{\mathbf{x}}_\mathrm{r}/\|\tilde{\mathbf{x}}_\mathrm{r}\| \in \mathbb{S}^3,\ \forall\, \tilde{\mathbf{x}}_\mathrm{r} \in \mathbb{T}_{\boldsymbol{\nu}_\mathrm{r}}\mathbb{S}^3,$$

respectively (see [25], [26]). As introduced in Section II-C, the gnomonic projection/retraction can be further derived w.r.t. the local basis from the matrix form of unit quaternions as

$$\boldsymbol{\tau}_\mathrm{r} = \mathcal{P}_{\boldsymbol{\nu}_\mathrm{r}}(\mathbf{x}_\mathrm{r}) = \mathcal{A}_{\mathbf{x}_\mathrm{r}}^{\llcorner\top} \mathbf{x}_\mathrm{r}/(\boldsymbol{\nu}_\mathrm{r}^\top \mathbf{x}_\mathrm{r}) \in \mathbb{R}^3,$$
$$\mathbf{x}_\mathrm{r} = \mathcal{U}_{\boldsymbol{\nu}_\mathrm{r}}(\boldsymbol{\tau}_\mathrm{r}) = \mathcal{Q}_{\mathbf{x}_\mathrm{r}}^\llcorner [1, \boldsymbol{\tau}_\mathrm{r}^\top]^\top / \sqrt{1 + \|\boldsymbol{\tau}_\mathrm{r}\|^2} \in \mathbb{S}^3.$$

Given the dual quaternion $\boldsymbol{\nu} = [\boldsymbol{\nu}_\mathrm{r}^\top, \boldsymbol{\nu}_\mathrm{s}^\top]^\top \in \mathbb{DH}_1$, the dual part is by definition located in the hyperspherical tangent space at the real part, i.e., $\boldsymbol{\nu}_\mathrm{s} \in \mathbb{T}_{\boldsymbol{\nu}_\mathrm{r}}\mathbb{S}^3$. This allows us to augment the tangent space $\mathbb{T}_{\boldsymbol{\nu}_\mathrm{r}}\mathbb{S}^3$ with the dual part via (4) w.r.t. the local basis. Such a locally augmented tangent space (LATS) is a six-dimensional Euclidean space and enables particle-wise quantification of the uncertainty on $\mathbb{DH}_1$. More specifically, we propose the augmented gnomonic projection

$$\boldsymbol{\tau} = \mathcal{P}_{\boldsymbol{\nu}_\mathrm{r}}^\oplus(\mathbf{x}) = [\boldsymbol{\tau}_\mathrm{r}^\top, \boldsymbol{\tau}_\mathrm{s}^\top]^\top \in \mathbb{R}^6, \forall\, \mathbf{x} = [\mathbf{x}_\mathrm{r}^\top, \mathbf{x}_\mathrm{s}^\top]^\top \in \mathbb{DH}_1,$$

with $\boldsymbol{\tau}_\mathrm{r} = \mathcal{P}_{\boldsymbol{\nu}_\mathrm{r}}(\mathbf{x}_\mathrm{r}) \in \mathbb{R}^3$, $\boldsymbol{\tau}_\mathrm{s} = \mathcal{R}_{\boldsymbol{\nu}_\mathrm{r}}^\top(\mathbf{t}_\mathbf{x} - \mathbf{t}_{\boldsymbol{\nu}}) \in \mathbb{R}^3$ being the mapped real and dual parts, respectively. $\mathcal{R}_{\boldsymbol{\nu}_\mathrm{r}}$ denotes the

Algorithm 1: DQ-UKF

Input: $(\boldsymbol{\nu}_{k-1}, \mathbf{C}_{k-1})$, measurement $\mathbf{z}_k$
Output: $(\boldsymbol{\nu}_k, \mathbf{C}_k)$
/* prediction step */
1 $\{(\boldsymbol{\tau}^i_{k-1}, v_i)\}^n_{i=1} \leftarrow \text{sampleUT}\,(\mathbf{C}_{k-1})$;
2 $\{\boldsymbol{\sigma}^i_{k-1}\}^n_{i=1} \leftarrow \text{augRetract}\,(\boldsymbol{\nu}_{\mathrm{r},k-1}, \{\boldsymbol{\tau}^i_{k-1}\}^n_{i=1})$;
3 $\{\boldsymbol{\sigma}^i_{k|k-1}\}^n_{i=1} \leftarrow \text{propagate}\,(\{\boldsymbol{\sigma}^i_{k-1}\}^n_{i=1})$;
4 $\boldsymbol{\nu}_{k|k-1} \leftarrow \text{average}\,(\{(\boldsymbol{\sigma}^i_{k|k-1}, v_i)\}^n_{i=1})$;
5 $\{\boldsymbol{\tau}^i_{k|k-1}\}^n_{i=1} \leftarrow \text{augProj}\,(\boldsymbol{\nu}_{\mathrm{r},k|k-1}, \{\boldsymbol{\sigma}^i_{k|k-1}\}^n_{i=1})$;
6 $\mathbf{C}_{k|k-1} \leftarrow \sum_i v_i\, \boldsymbol{\tau}^i_{k|k-1} (\boldsymbol{\tau}^i_{k|k-1})^\top$;
7 $\{\mathbf{z}^i_{k|k-1}\}^n_{i=1} \leftarrow \text{measure}\,(\{\boldsymbol{\sigma}^i_{k|k-1}\}^n_{i=1})$;
/* update step */
8 $\bar{\mathbf{z}}_{k|k-1} \leftarrow \sum_i v_i\, \mathbf{z}^i_{k|k-1}$;
9 $\mathbf{C}_{\mathbf{z}} \leftarrow \sum_i v_i (\mathbf{z}^i_{k|k-1} - \bar{\mathbf{z}}_{k|k-1})(\mathbf{z}_{k|k-1} - \bar{\mathbf{z}}_{k|k-1})^\top$;
10 $\mathbf{C}_{\boldsymbol{\tau}\mathbf{z}} \leftarrow \sum_i v_i\, \boldsymbol{\tau}^i_{k|k-1} (\mathbf{z}^i_{k|k-1} - \bar{\mathbf{z}}_{k|k-1})^\top$;
11 $\mathbf{K}_k \leftarrow \mathbf{C}_{\boldsymbol{\tau}\mathbf{z}} (\mathbf{C}_{\mathbf{z}})^{-1}$;
12 $\boldsymbol{\tau}_k \leftarrow \mathbf{K}_k (\mathbf{z}_k - \bar{\mathbf{z}}_{k|k-1})$;
13 $\mathbf{C}_k \leftarrow \mathbf{C}_{k|k-1} - \mathbf{K}_k\, \mathbf{C}_{\mathbf{z}}\, \mathbf{K}_k^\top$;
14 $\boldsymbol{\nu}_k \leftarrow \text{augRetract}\,(\boldsymbol{\nu}_{\mathrm{r},k|k-1}, \boldsymbol{\tau}_k)$;
15 **return** $(\boldsymbol{\nu}_k, \mathbf{C}_k)$

rotation matrix given by the real part $\boldsymbol{\nu}_\mathrm{r}$. A detailed derivation for the mapped dual part $\boldsymbol{\tau}_\mathrm{s}$ is given in the Appendix. Inversely, the augmented gnomonic retraction is

$$\mathbf{x} = \mathcal{U}^{\oplus}_{\boldsymbol{\nu}_\mathrm{r}}(\boldsymbol{\tau}) = [\mathbf{x}_\mathrm{r}^\top, \mathbf{x}_\mathrm{s}^\top]^\top \in \mathbb{DH}_1, \forall\, \boldsymbol{\tau} = [\boldsymbol{\tau}_\mathrm{r}^\top, \boldsymbol{\tau}_\mathrm{s}^\top]^\top \in \mathbb{R}^6,$$

with $\mathbf{x}_\mathrm{r} = \mathcal{U}_{\boldsymbol{\nu}_\mathrm{r}}(\boldsymbol{\tau}_\mathrm{r}) \in \mathbb{S}^3$, $\mathbf{x}_\mathrm{s} = 0.5\, \mathcal{A}^{\lrcorner}_{\mathbf{x}_\mathrm{r}}(\mathcal{R}_{\boldsymbol{\nu}_\mathrm{r}} \boldsymbol{\tau}_\mathrm{s} + \mathbf{t}_{\boldsymbol{\nu}}) \in \mathbb{T}_{\mathbf{x}_\mathrm{r}}\mathbb{S}^3$.

In order to estimate the proposal distribution in (5) with a UKF-like scheme, a six-dimensional Gaussian distribution is deployed in the LATS at each particle on the manifold $\mathbb{DH}_1$. As discussed in [25], points on the hypersphere are unbounded in the tangent space after being mapped via the gnomonic projection. Therefore, sigma points in the LATS ($\mathbb{R}^6$ w.r.t. its local basis) can always be mapped back to $\mathbb{DH}_1$ via the proposed augmented gnomonic retraction.

IV. Unscented Dual Quaternion Particle Filter (DQ-UPF)

Based on the stochastic modeling of dual quaternions in Section III, we propose a UKF on manifold $\mathbb{DH}_1$ for estimating the proposal distribution in a particle-wise manner (shown in Alg. 1). For each particle, sigma points $\{\boldsymbol{\tau}^i_{k-1}\}^n_{i=1} \subset \mathbb{R}^6$ are first drawn in the LATS at last posterior real part $\boldsymbol{\nu}_{\mathrm{r},k-1}$ with its covariance $\mathbf{C}_{k-1}$ based on unscented transform. They are then mapped back to the manifold via the augmented gnomonic retraction and propagated through the system dynamics (Alg. 1, lines 1–3). The mean value of the propagated dual quaternion samples is calculated by averaging the translation and rotation components separately. The real parts $\{\boldsymbol{\sigma}^i_{\mathrm{r},k|k-1}\}^n_{i=1}$ are averaged by the intrinsic gradient descent from [27] with an adaptation to the hyperspherical gnomonic projection. The LATS is then transported to the prior real part $\boldsymbol{\nu}_{\mathrm{r},k|k-1}$, where the prior covariance $\mathbf{C}_{k|k-1}$ is computed (Alg. 1, lines 5–6). Further, we perform the UKF update

Algorithm 2: U-DQPF

Input: $\{(\boldsymbol{\nu}^i_{k-1}, w^i_{k-1}, \mathbf{C}^i_{k-1})\}^n_{i=1}$, measurement $\mathbf{z}_k$
Output: $\{(\boldsymbol{\nu}^i_k, w^i_k, \mathbf{C}^i_k)\}^n_{i=1}$
1 **for** $i \leftarrow 1$ **to** n **do**
/* particle-wise DQ-UKF */
2 $(\boldsymbol{\nu}^i_k, \mathbf{C}^i_k) \leftarrow \text{DQ-UKF}(\boldsymbol{\nu}^i_{k-1}, \mathbf{C}^i_{k-1})$;
/* importance weighting */
3 $\hat{\boldsymbol{\tau}}^i_k \leftarrow \text{sampleRnd}\,(\mathcal{N}(\mathbf{0}, \mathbf{C}^i_k))$;
4 $\hat{\mathbf{x}}^i_k \leftarrow \text{augRetract}\,(\boldsymbol{\nu}^i_{\mathrm{r},k}, \hat{\boldsymbol{\tau}}^i_k)$;
5 $w^i_k \leftarrow w^i_{k-1} \frac{f^{\mathrm{L}}(\mathbf{z}_k \,|\, \hat{\mathbf{x}}^i_k) f^{\mathrm{T}}(\hat{\mathbf{x}}^i_k \,|\, \mathbf{x}^i_{k-1})}{g(\hat{\mathbf{x}}^i_k \,|\, \mathbf{x}^i_{0:k-1}, \mathbf{z}_{1:k})}$;
6 $\{w^i_k\}^n_{i=1} \leftarrow \text{normalize}(\{w^i_k\}^n_{i=1})$;
7 $\{(\boldsymbol{\nu}^i_k, w^i_k, \mathbf{C}^i_k)\}^n_{i=1} \leftarrow \text{resample}(\{(\boldsymbol{\nu}^i_k, w^i_k, \mathbf{C}^i_k)\}^n_{i=1})$;
8 **return** $\{(\boldsymbol{\nu}^i_k, w^i_k, \mathbf{C}^i_k)\}^n_{i=1}$

to fuse the measurement $\mathbf{z}_k$ on the LATS at the prior real part $\boldsymbol{\nu}_{\mathrm{r},k|k-1}$ w.r.t. to its local basis (Alg. 1, lines 7–13). In the end, the posterior state $\boldsymbol{\tau}_k$ in the tangent space is retracted back to the manifold $\mathbb{DH}_1$ to obtain the state $\boldsymbol{\nu}_k$.

The proposed DQ-UKF is further integrated into the unscented particle filtering scheme from [22] to obtain the proposal distribution particle-wise (Alg. 2, line 2). Afterward, a random sample $\boldsymbol{\tau}^i_k$ is drawn in the LATS at the posterior $\boldsymbol{\nu}^i_{\mathrm{r},k}$. There, the proposal density $g(\hat{\mathbf{x}}_i \,|\, \mathbf{x}^i_{0:k-1}, \mathbf{z}_{1:k})$ is evaluated according to the Gaussian distribution $\mathcal{N}(\mathbf{0}, \mathbf{C}^i_k)$. The random sample in the tangent space $\boldsymbol{\tau}^i_k$ is then retracted back to the manifold to compute the likelihood $f(\mathbf{z}_k \,|\, \hat{\mathbf{x}}^i_k)$ as well as the transition density in the LATS at the prior real part $\boldsymbol{\nu}^i_{\mathrm{r},k|k-1}$ (Alg. 2, lines 3–4). Then, the weights of all particles are updated according to (5) and re-normalized. As suggested in [24], a resampling is performed to obtain uniformly weighted particles (Alg. 2, lines 5–7).

V. Evaluation

The proposed U-DQPF is evaluated in a simulation. We set up the system model as $\mathbf{x}_{k+1} = \mathbf{x}_k \boxplus \mathbf{w}^2_k$. $\mathbf{x}_{k+1}, \mathbf{x}_k \in \mathbb{DH}_1$ denote the dual quaternion states representing spatial poses. $\mathbf{w}_k = [\mathbf{w}^\top_{\mathrm{r},k}, \mathbf{w}^\top_{\mathrm{s},k}]^\top \in \mathbb{DH}_1$ is the uncertain system input with $\mathbf{w}_{\mathrm{r},k} = [\cos(\theta_{\mathbf{w},k}/2), \mathbf{n}^\top_{\mathbf{w},k} \sin(\theta_{\mathbf{w},k}/2)]^\top$ and $\mathbf{w}_{\mathrm{s},k} = 0.5\,[0, \mathbf{t}^\top_{\mathbf{w},k}]^\top \otimes \mathbf{w}_{\mathrm{r},k}$ being the real and dual parts, respectively. $\mathbf{w}^2_k$ is defined as $\mathbf{w}_k \boxplus \mathbf{w}_k$. We assume the uncertain rotation angle to be von Mises-distributed and the rotation axis von Mises–Fisher-distributed [11], i.e., $\theta_{\mathbf{w},k} \sim \mathcal{VM}(\phi^\theta_\mathbf{w}, \kappa^\theta_\mathbf{w})$ and $\mathbf{n}_{\mathbf{w},k} \sim \mathcal{VMF}(\boldsymbol{\zeta}^\mathbf{n}_\mathbf{w}, \kappa^\mathbf{n}_\mathbf{w})$. The mean values of the rotation angle and axis are $\phi^\theta_\mathbf{w} = \pi/6$ and $\boldsymbol{\zeta}^\mathbf{n}_\mathbf{w} = [1/\sqrt{3}, 1/\sqrt{3}, 1/\sqrt{3}]^\top$, respectively. The concentrations are $\kappa^\theta_\mathbf{w} = \kappa^\mathbf{n}_\mathbf{w} = 100$. The uncertain translation input is state-dependent with $\mathbf{t}_{\mathbf{w},k} = (1 - \mathbf{x}_{k,0})\, \tilde{\mathbf{t}}_k$, where $\mathbf{x}_{k,0}$ is the first element of state $\mathbf{x}_k$. The external input $\tilde{\mathbf{t}}_k$ is Gaussian-distributed, i.e., $\tilde{\mathbf{t}}_k \sim \mathcal{N}(\boldsymbol{\mu}^{\tilde{\mathbf{t}}}_\mathbf{w}, \boldsymbol{\Sigma}^{\tilde{\mathbf{t}}}_\mathbf{w})$ with $\boldsymbol{\mu}^{\tilde{\mathbf{t}}}_\mathbf{w} = [10, 10, 10]^\top$ and $\boldsymbol{\Sigma}^{\tilde{\mathbf{t}}}_\mathbf{w} = 0.1 \cdot \mathbf{I}_{3\times3}$. The measurement model is

$$\mathbf{z}_k = \left(\mathbf{x}_k \boxplus [1, 0, 0, 0, 0, \mathbf{z}_0]^\top \boxplus \mathbf{x}^{\odot}_k\right)_{6:8} + \mathbf{v}_k, \tag{6}$$

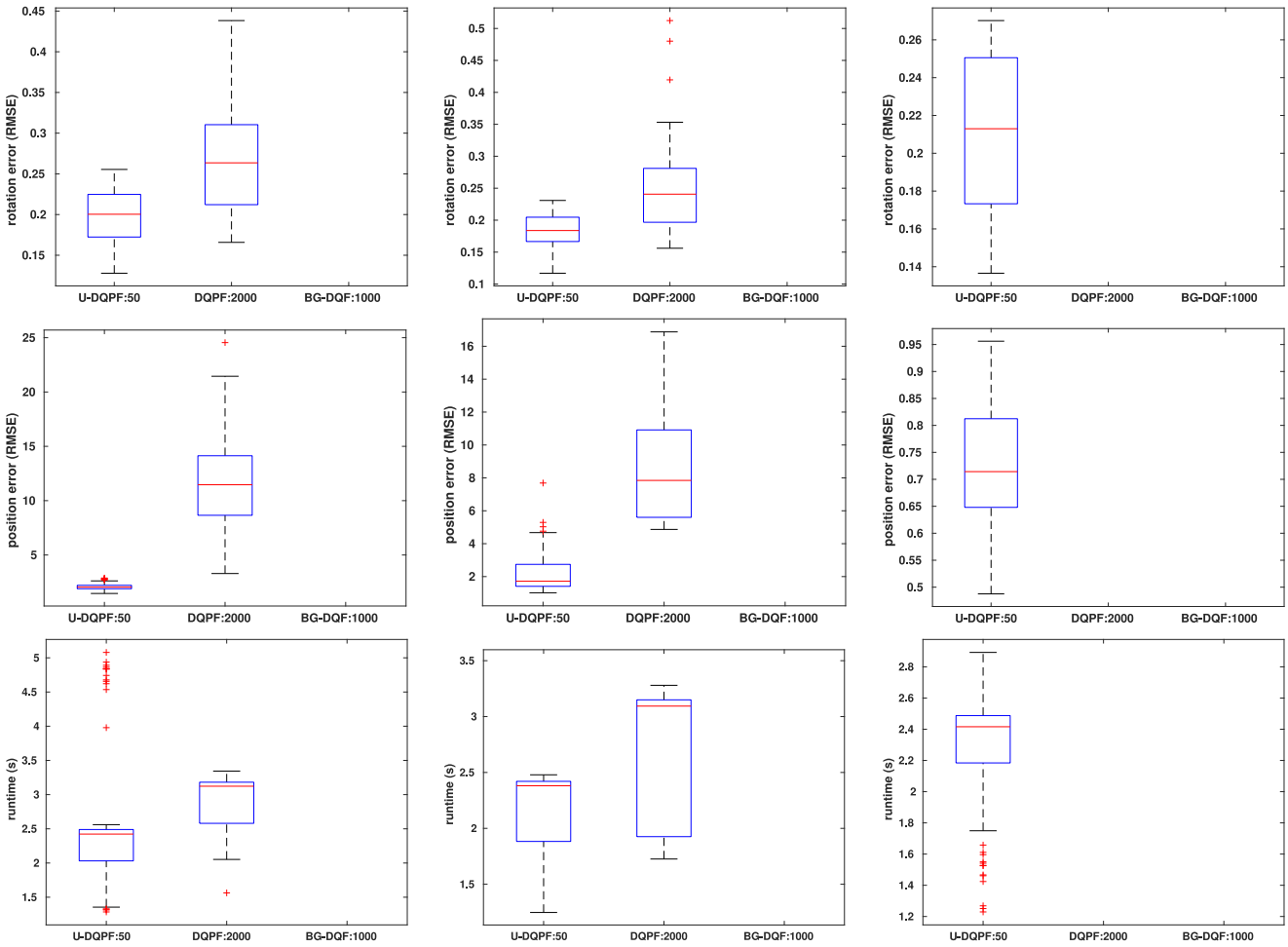

(a) large noise ($\lambda_{\mathrm{DQPF}} = 59\%$) (b) medium noise ($\lambda_{\mathrm{DQPF}} = 76\%$) (c) low noise ($\lambda_{\mathrm{DQPF}} = 100\%$)

Fig. 1. Comparison of the unscented dual quaternion particle filter with existing dual quaternion filters (using `boxplot` in MATLAB). The whiskers are limited to 2.7 standard deviations from the median. The lack of a box indicates a total tracking failure. The U-DQPF gives superior accuracy, efficiency and robustness under different measurement noise levels.

with $\mathbf{z}_k$ denoting the coordinates of a point transformed by state $\mathbf{x}_k$ from its initial coordinates $\mathbf{z}_0 = [1, 2, 1]^\top \in \mathbb{R}^3$.

As a comparison, a standard dual quaternion particle filter (DQPF) is implemented with the transition density being the proposal distribution in (5). Also, the parametric approach for modeling uncertain dual quaternions from [8] is employed, in which the real part is assumed to be Bingham-distributed and the translation to be Gaussian-distributed. We further enhance this Bingham–Gaussian dual quaternion filter (BG-DQF) with the deterministic sampling approaches from [25] and [28]. Compared with the standard unscented transform-based scheme, they enable deterministic sampling with user-configurable numbers of quaternion and translation samples, further facilitating nonlinear filterings. For the proposed U-DQPF, 50 particles are deployed, whereas the DQPF uses 2000 particles, and the BG-DQF relies on 1000 deterministic samples. We perform the evaluation under different noise levels for the measurement model in (6), where $\mathbf{\Sigma}_{\mathbf{v}}^{\mathbf{t}} = \alpha\, \mathbf{I}_{3\times 3}$, with $\alpha \in \{1, 0.5, 0.05\}$. Moreover, for all the three noise levels, 100 Monte Carlo runs are performed with 20 time steps each. We compute the rotation error as the quaternion arc length (considering symmetry) on $\mathbb{S}^3$ and the translation error as the Euclidean distance in $\mathbb{R}^3$.

The parametric model-based BG-DQF fails to perform the tracking task for all three noise levels due to the highly nonlinear system dynamics and violation of the parametric assumption of Bingham–Gaussian uncertainty (see Fig. 1). The conventional PF suffers from sample degeneration issues as it neglects the latest observed evidence under the high nonlinearity (failure rate denoted by λ_{DQPF}). Also, the PF shows deteriorated tracking accuracy when the likelihood function becomes peakier (i.e., for lower measurement noise levels). In the case of the low measurement noise level (e.g., obtained from highly accurate sensors) with $\alpha = 0.05$, the DQPF totally loses tracking. In contrast, the proposed U-DQPF shows no failure and achieves a higher tracking accuracy and efficiency than the other filters for all three noise levels.

There are a few outliers in the runtime plots with the proposed filter. This mainly results from the variable convergence speed when averaging the quaternion samples using the intrinsic gradient descent algorithm from [27]. Furthermore, the estimates shown in the plot are computed based on

separately averaged quaternion and translation components. Averaging approaches on manifolds are still actively studied. Thus, the U-DQPF can be further improved by introducing a unified averaging approach that is adaptive to the unit dual quaternion manifold.

VI. Conclusion

We propose a conceptual framework for recursive estimation of rigid body motions, namely, the unscented dual quaternion particle filter (U-DQPF). Dual quaternion particles enable exact modeling of arbitrary distributions on SE(3) group. A novel UKF-like filtering scheme is established adaptive to the manifold structure and performed particle-wise to estimate the proposal distribution. Thus, the latest observed evidence is fused for importance sampling, resulting in considerable improvement over existing dual quaternion filters using parametric modeling as well as a plain Monte Carlo scheme. In practical applications in which inertial sensors are available, extra motion information, e.g., velocities, can be integrated into the locally augmented tangent space. The proposed framework can then be extended for joint estimation of enlarged state vectors to handle highly dynamic tracking tasks. Also, the proposed U-DQPF should be deployed to various real-world scenarios to validate its superior performance [8], [14].

Appendix
Augmented Gnomonic Projection on $\mathbb{DH}_1$

When mapping any dual quaternion $\mathbf{x} = [\mathbf{x}_\mathrm{r}^\top, \mathbf{x}_\mathrm{s}^\top]^\top \in \mathbb{DH}_1$ to the LATS at $\boldsymbol{\nu} = [\boldsymbol{\nu}_\mathrm{r}^\top, \boldsymbol{\nu}_\mathrm{s}^\top]^\top \in \mathbb{DH}_1$ via augmented gnomonic projection, the mapped dual part is essentially the subtracted translation term. As in [16], it can be derived as

$$\boldsymbol{\Delta} = [\boldsymbol{\Delta}_\mathrm{r}^\top, \boldsymbol{\Delta}_\mathrm{s}^\top]^\top := \boldsymbol{\nu}^{-1} \boxplus \mathbf{x} = \begin{bmatrix} \boldsymbol{\nu}_\mathrm{r}^{-1} \otimes \mathbf{x}_\mathrm{r} \\ \boldsymbol{\nu}_\mathrm{r}^{-1} \otimes \mathbf{x}_\mathrm{s} + \boldsymbol{\nu}_\mathrm{s}^* \otimes \mathbf{x}_\mathrm{r} \end{bmatrix},$$

from which the translation can be derived via (4) as

$$\begin{aligned} \left[0, \mathbf{t}_{\boldsymbol{\Delta}}^\top\right]^\top &= 2\,(\boldsymbol{\nu}_\mathrm{r}^{-1} \otimes \mathbf{x}_\mathrm{s} + \boldsymbol{\nu}_\mathrm{s}^* \otimes \mathbf{x}_\mathrm{r}) \otimes (\boldsymbol{\nu}_\mathrm{r}^{-1} \otimes \mathbf{x}_\mathrm{r})^{-1} \\ &= 2\,(\boldsymbol{\nu}_\mathrm{r}^{-1} \otimes \mathbf{x}_\mathrm{s} + \boldsymbol{\nu}_\mathrm{s}^* \otimes \mathbf{x}_\mathrm{r}) \otimes \mathbf{x}_\mathrm{r}^{-1} \otimes \boldsymbol{\nu}_\mathrm{r} \\ &= 2\,\boldsymbol{\nu}_\mathrm{r}^{-1} \otimes \mathbf{x}_\mathrm{s} \otimes \mathbf{x}_\mathrm{r}^{-1} \otimes \boldsymbol{\nu}_\mathrm{r} + 2\,\boldsymbol{\nu}_\mathrm{s}^* \otimes \boldsymbol{\nu}_\mathrm{r} \\ &= \boldsymbol{\nu}_\mathrm{r}^{-1} \otimes [0, \mathbf{t}_\mathbf{x}^\top]^\top \otimes \boldsymbol{\nu}_\mathrm{r} + \boldsymbol{\nu}_\mathrm{r}^* \otimes [0, -\mathbf{t}_{\boldsymbol{\nu}}^\top]^\top \otimes \boldsymbol{\nu}_\mathrm{r} \\ &= \boldsymbol{\nu}_\mathrm{r}^{-1} \otimes [0, \mathbf{t}_\mathbf{x}^\top - \mathbf{t}_{\boldsymbol{\nu}}^\top]^\top \otimes \boldsymbol{\nu}_\mathrm{r}. \end{aligned}$$

Therefore, we obtain $\mathbf{t}_{\boldsymbol{\Delta}} = \mathcal{R}_{\boldsymbol{\nu}_\mathrm{r}^{-1}}(\mathbf{t}_\mathbf{x} - \mathbf{t}_{\boldsymbol{\nu}}) = \mathcal{R}_{\boldsymbol{\nu}_\mathrm{r}}^\top(\mathbf{t}_\mathbf{x} - \mathbf{t}_{\boldsymbol{\nu}})$.

References

[1] D. Choukroun and Y. Zivan, "Vision-aided spacecraft relative pose estimation via dual quaternions," in *Proc. 58th IEEE Conf. Decis. Control (CDC)*, Nice, France, Dec. 2019, pp. 7893–7898.

[2] J. Engel, J. Sturm, and D. Cremers, "Camera-based navigation of a low-cost quadrocopter," in *Proc. IEEE/RSJ Int. Conf. Intell. Robots Syst. (IROS)*, Vilamoura, Portugal, Oct. 2012, pp. 2815–2821.

[3] H. A. Hashim, L. J. Brown, and K. McIsaac, "Nonlinear stochastic position and attitude filter on the special euclidean group 3," *J. Franklin Inst.*, vol. 356, no. 7, pp. 4144–4173, 2019.

[4] H. A. Hashim, L. J. Brown, and K. McIsaac, "Nonlinear pose filters on the special Euclidean Group SE(3) with guaranteed transient and steady-state performance," *IEEE Trans. Syst., Man, Cybern., Syst.*, early access, Jun. 13, 2019, doi: 10.1109/TSMC.2019.2920114.

[5] H. A. Hashim and F. L. Lewis, "Nonlinear stochastic estimators on the special Euclidean group SE(3) using uncertain IMU and vision measurements," *IEEE Trans. Syst., Man, Cybern., Syst.*, early access, Mar. 23, 2020, doi: 10.1109/TSMC.2020.2980184.

[6] S. J. Julier and J. K. Uhlmann, "Unscented filtering and nonlinear estimation," *Proc. IEEE*, vol. 92, no. 3, pp. 401–422, Mar. 2004.

[7] S. Hauberg, F. Lauze, and K. S. Pedersen, "Unscented Kalman filtering on Riemannian manifolds," *J. Math. Imag. Vis.*, vol. 46, no. 1, pp. 103–120, 2013.

[8] S. Bultmann, K. Li, and U. D. Hanebeck, "Stereo visual SLAM based on unscented dual quaternion filtering," in *Proc. 22nd Int. Conf. Inf. Fusion (Fusion)*, Ottawa, ON, Canada, Jul. 2019, pp. 1–8.

[9] R. Arun Srivatsan, M. Xu, N. Zevallos, and H. Choset, "Probabilistic pose estimation using a bingham distribution-based linear filter," *Int. J. Robot. Res.*, vol. 37, nos. 13–14, pp. 1610–1631, 2018.

[10] J. Glover and L. P. Kaelbling, "Tracking the spin on a ping pong ball with the quaternion bingham filter," in *Proc. IEEE Int. Conf. Robot. Autom. (ICRA)*, Hong Kong, China, May 2014, pp. 4133–4140.

[11] K. V. Mardia and P. E. Jupp, *Directional Statistics*, vol. 494. New York, NY, USA: Wiley, 2009,

[12] M. L. Psiaki, "Estimation using quaternion probability densities on the unit hypersphere," *J. Astronaut. Sci.*, vol. 54, nos. 3–4, pp. 415–431, 2006.

[13] I. Gilitschenski, G. Kurz, S. J. Julier, and U. D. Hanebeck, "Unscented orientation estimation based on the Bingham distribution," *IEEE Trans. Autom. Control*, vol. 61, no. 1, pp. 172–177, Jan. 2016.

[14] R. A. Srivatsan, G. T. Rosen, D. F. N. Mohamed, and H. Choset, "Estimating SE(3) elements using a dual quaternion based linear Kalman filter," in *Proc. Robot. Sci. Syst. (RSS)*, Boston, MA, USA, 2016.

[15] I. Gilitschenski, G. Kurz, S. J. Julier, and U. D. Hanebeck, "A new probability distribution for simultaneous representation of uncertain position and orientation," in *Proc. 17th Int. Conf. Inf. Fusion (Fusion)*, Salamanca, Spain, Jul. 2014, pp. 1–7.

[16] K. Li, F. Pfaff, and U. D. Hanebeck, "Geometry-driven stochastic modeling of SE(3) states based on dual quaternion representation," in *Proc. IEEE Int. Conf. Multisens. Fusion Integr. Intell. Syst. (MFI)*, Taipei, Taiwan, May 2019, pp. 254–260.

[17] W. Feiten, P. Atwal, R. Eidenberger, and T. Grundmann, "6D pose uncertainty in robotic perception," in *Advances in Robotics Research*. Heidelberg, Germany: Springer, 2009, pp. 89–98.

[18] W. Feiten and M. Lang, "MPG—A framework for reasoning on 6 DoF pose uncertainty," 2017. [Online]. Available: arXiv:1707.01941.

[19] J. Glover, G. Bradksi, and R. Rusu, "Monte Carlo pose estimation with quaternion kernels and the Bingham distribution," in *Proc. Robot. Sci. Syst.*, Los Angeles, CA, USA, Jun. 2012.

[20] K. Li, F. Pfaff, and U. D. Hanebeck, "Grid-based quaternion filter for SO(3) estimation," in *Proc. Eur. Control Conf. (ECC)*, Saint Petersburg, Russia, May 2020.

[21] G. Kurz, F. Pfaff, and U. D. Hanebeck, "Application of discrete recursive Bayesian estimation on intervals and the unit circle to filtering on SE(2)," *IEEE Trans. Ind. Informat.*, vol. 14, no. 3, pp. 1197–1206, Mar. 2018.

[22] R. Van Der Merwe, A. Doucet, N. De Freitas, and E. A. Wan, "The unscented particle filter," in *Proc. Adv. Neural Inf. Process. Syst.*, 2001, pp. 584–590.

[23] B. Busam, T. Birdal, and N. Navab, "Camera pose filtering with local regression geodesics on the Riemannian manifold of dual quaternions," in *Proc. IEEE Int. Conf. Comput. Vis. Workshops*, Venice, Italy, 2017, pp. 2436–2445.

[24] M. S. Arulampalam, S. Maskell, N. Gordon, and T. Clapp, "A tutorial on particle filters for online nonlinear/non-Gaussian Bayesian tracking," *IEEE Trans. Signal Process.*, vol. 50, no. 2, pp. 174–188, Feb. 2002.

[25] K. Li, F. Pfaff, and U. D. Hanebeck, "Hyperspherical deterministic sampling based on Riemannian geometry for improved nonlinear Bingham filtering," in *Proc. 22nd Int. Conf. Inf. Fusion (Fusion)*, Ottawa, ON, Canada, Jul. 2019, pp. 1–8.

[26] P.-A. Absil and J. Malick, "Projection-like retractions on matrix manifolds," *SIAM J. Optim.*, vol. 22, no. 1, pp. 135–158, 2012.

[27] E. Kraft, "A quaternion-based unscented Kalman filter for orientation tracking," in *Proc. 6th Int. Conf. Inf. Fusion (Fusion)*, vol. 1. Cairns, QLD, Australia, 2003, pp. 47–54.

[28] J. Steinbring and U. D. Hanebeck, "LRKF revisited: The smart sampling Kalman filter (S2KF)," *J. Adv. Inf. Fusion*, vol. 9, no. 2, pp. 106–123, Dec. 2014.